Kinetically reduced local Navier-Stokes equations for simulation of incompressible viscous flows

S. Borok,[1] S. Ansumali,[1,*] and I. V. Karlin[2,3,†]

[1]*Division of Chemical and Biomolecular Engineering, Nanyang Technological University, 637459 Singapore*

[2]*Aerothermochemistry and Combustion Systems Lab, ETH Zurich, 8092 Zurich, Switzerland*

[3]*School of Engineering Sciences, University of Southampton, SO17 1BJ Southampton, United Kingdom*

(Received 23 July 2007; revised manuscript received 2 October 2007; published 10 December 2007)

Recently, another approach to study incompressible fluid flow was suggested [S. Ansumali, I. Karlin, and H. Öttinger, Phys. Rev. Lett. **94**, 080602 (2005)]—the kinetically reduced local Navier-Stokes (KRLNS) equations. We consider a simplified two-dimensional KRLNS system and compare it with Chorin's artificial compressibility method. A comparison of the two methods for steady state computation of the flow in a lid-driven cavity at various Reynolds numbers shows that the results from both methods are in good agreement with each other. However, in the transient flow, it is demonstrated that the KRLNS equations correctly describe the time evolution of the velocity and of the pressure, unlike the artificial compressibility method.

DOI: 10.1103/PhysRevE.76.066704 PACS number(s): 47.11.−j, 05.70.Ln

I. INTRODUCTION

The classical incompressible Navier-Stokes (INS) equations consist of the equation for the velocity [1]

$$\partial_t u_\alpha + u_\beta \partial_\beta u_\alpha + \partial_\alpha P = \frac{1}{\mathrm{Re}} \partial_\beta \partial_\beta u_\alpha, \tag{1}$$

and the incompressibility constraint

$$\partial_\alpha u_\alpha = 0, \tag{2}$$

where **u** is the fluid velocity, P is the pressure, and Re is the Reynolds number, which characterizes the relative strength of the viscous and the inertial forces. A well known difficulty in solving the system (1) and (2) numerically is the absence of time evolution equation for the pressure. The pressure is not an independent variable, and it must be determined so that the incompressibility condition (2) is satisfied. In many numerical schemes the pressure is obtained by solving a Poisson equation, which is often the most costly step in simulations.

Therefore, alternative physical models of incompressibility have been explored. To date, the most successful approach is the lattice Boltzmann method (LBM) [2]. The LBM models are derived from the Boltzmann equation under the assumption of a low Mach number [3,4], and provide a viable alternative to computational fluid dynamics (CFD) methods for practical applications [5]. However, certain features pertinent to the LBM (a relatively large number of fields and fixed uniform grids) impose limitations, which so far persist in spite of numerous attempts.

Another technique to avoid solving the Poisson equation was suggested by Chorin in the classical paper [8], and is known as the artificial compressibility (AC) method. The basic idea of this formulation is to introduce the time derivative of the pressure into the continuity equation thereby providing a direct coupling between the pressure and the velocity. Thus, in this method, the continuity equation (2) is replaced by

$$\partial_t P = -\frac{1}{\delta} \partial_\alpha u_\alpha, \tag{3}$$

where δ is the artificial compressibility parameter, $P=\rho/\delta$ (ρ-density) is the artificial equation of state, and t is an auxiliary variable that can be related to the physical time. The parameter δ depends on a problem under study and should be chosen such that the convergence to the steady state is reached as fast as possible. For the system (1) and (3) an artificial sound speed c is defined as $c=1/\sqrt{\delta}$ [8]. It is shown (see, for example, [9] and the references therein) that solutions of the system (1) and (3) converge to steady state solution of INS equations (1) and (2). In order to compare the unsteady solution of the AC method with the solution obtained from INS equation, the parameter δ should be chosen sufficiently small. However, in practice, the method is numerically efficient only when moderate values of δ is chosen. For such values of δ, the time dependent behavior is not accurate. Many modifications of the Chorin method were suggested in order to compute accurate solutions, see for example [10,11].

Recently, an alternative thermodynamic description of incompressible fluid flows was suggested in the form of kinetically reduced local Navier-Stokes (KRLNS) equations [6]. The starting point in Ref. [6] was the set of compressible (local) Navier-Stokes equations for the density ρ, the momentum density $\boldsymbol{m}=\rho\boldsymbol{u}$, and the negative of the grand potential $\mathcal{G}$,

$$\mathcal{G} = P - \frac{m^2}{2\rho}. \tag{4}$$

Here, P is the (local) thermodynamic pressure measured in a comoving (Lagrange) coordinate system. It was shown that, after the acoustic (density) mode is damped out on the short time and length scales,

*asantosh@ntu.edu.sg

†karlin.ilya@gmail.com

$$t_a \sim \sqrt{\mathrm{Kn}}\mathrm{Ma}T, \quad l_a \sim \sqrt{\mathrm{Kn}}L, \tag{5}$$

respectively, where L is a characteristic flow length scale, T is the flow time scale, one arrives at a coupled system of equations for the nondimensional momentum density $\boldsymbol{j}=\boldsymbol{m}/(\bar{\rho}U_0)$, where $\bar{\rho}U_0$ is a characteristic momentum (known from the initial or boundary conditions), and the nondimensional grand potential density $\Theta=\mathcal{G}/(\bar{\rho}U_0^2)$. In Eq. (5), the Mach number, $\mathrm{Ma}=U_0/c_s$, is the ratio of the characteristic flow velocity U_0 to the isentropic sound speed c_s, and the Knudsen number, $\mathrm{Kn}=\mu/(\rho c_s L)$, is the ratio of the sound propagation time L/c_s, to the momentum diffusivity time. In the KRLNS equations [6], the fast dynamics of the grand potential becomes singularly coupled to the slow dynamics of momentum, and the incompressible Navier-Stokes equations are the quasistationary solution of the KRLNS equations at small Mach number. Further applications of the KRLNS equations were presented in Ref. [7]. We extend that work in the present paper with the aim to: apply the KRLNS equations for such a well known problem as a flow in a square cavity and compare the results with those available in the literature and compare the KRLNS equation with the AC method for both steady-state (flow in a cavity) and transient flow problems.

The outline of the paper is as follows. In Sec. II the simplified KRLNS equations are discussed. In Sec. III we rescale the KRLNS system (written in terms of momentum-grand potential density) into the original variables (velocity-pressure), in order to have the same units as AC and INS for a further comparison. In Sec. IV we discuss the numerical results. Section V concludes the work. In Appendix A, the details of the numerical method are given while in Appendix B, a characteristic analysis of the advection term of the KRLNS equation is presented.

II. KRLNS EQUATIONS

We consider a simplified version of the KRLNS equations which contain the terms required to reconstruct the INS equations as the quasistationary approximation. Here we recall the steps needed for this simplification as they were formulated in [7].

The equation for the dimensionless grand potential density Θ [Eq. (10) in Ref. [6]] is a diffusion equation with a source term, which depends solely on the dimensionless momentum $\boldsymbol{j}$,

$$\partial_t\Theta - \sqrt{\mathrm{Kn}}\frac{\gamma}{\mathrm{Pr}}\partial_\alpha\partial_\alpha\Theta = -\frac{1}{\mathrm{Ma}}\partial_\alpha j_\alpha + F(\boldsymbol{j}), \tag{6}$$

where γ is the adiabatic exponent, Pr is the Prandtl number, and F is the nonlinear part of the source term,

$$F = \mathrm{Ma}\partial_\alpha\left(\frac{j_\alpha j^2}{2}\right) + \sqrt{\mathrm{Kn}}\left[\left(\frac{\gamma}{\mathrm{Pr}}-1\right)\partial_\alpha\partial_\alpha\frac{j^2}{2} + (\partial_\alpha j_\beta)(\partial_\alpha j_\beta)\right.$$
$$+ \left.\frac{\partial P}{\partial T}\bigg|_{\bar{\rho}}\frac{1}{2C_V}(\partial_\alpha j_\beta + \partial_\beta j_\alpha)(\partial_\alpha j_\beta + \partial_\beta j_\alpha)\right.$$
$$\left. - \left(1+\lambda-\frac{2}{D}\right)\partial_\beta(j_\beta\partial_\alpha j_\alpha)\right]. \tag{7}$$

In the sequel, we neglect the nonlinear term F, and retain only the leading order source term, $\mathrm{Ma}^{-1}\partial_\alpha j_\alpha$, $\mathrm{Ma}\ll 1$, responsible for maintaining incompressibility. As was explained in Ref. [6], the use of the grand potential is crucial in the KRLNS equations since any other choice of the thermodynamic function (e.g., of the entropy S) would immediately lead to an advection term, $j_\alpha\partial_\alpha S$, and in a nontrivial coupling to the momentum equation. Finally, although not strictly necessary, we shall also set $\mathrm{Pr}=\gamma$.

The momentum equation [Eq. (10) in Ref. [6]] reads

$$\partial_t j_\alpha = -\mathrm{Ma}j_\alpha\partial_\beta j_\beta - \mathrm{Ma}j_\beta\partial_\beta j_\alpha - \mathrm{Ma}\partial_\alpha\left(\Theta+\frac{j^2}{2}\right)$$
$$+ \sqrt{\mathrm{Kn}}\left(1+\lambda-\frac{2}{D}\right)\partial_\alpha\partial_\beta j_\beta + \sqrt{\mathrm{Kn}}\partial_\beta\partial_\beta j_\alpha, \tag{8}$$

where λ is a ratio of bulk viscosity to shear viscosity. In (8) we shall neglect the bulk viscosity term, which is proportional to the divergence, $\sim\sqrt{\mathrm{Kn}}\partial_\alpha\partial_\beta j_\beta$, as compared to the first term in the right-hand side, $-\mathrm{Ma}j_\alpha\partial_\beta j_\beta$. This is consistent with the assumption $\mathrm{Kn}\ll\mathrm{Ma}$ under which the KRLNS equations were derived. Eventually, both these terms could be neglected because we expect (this was confirmed in [7]) that the divergence itself is of the order Ma. However, we shall retain the first term in the right-hand side of Eq. (8) in order to achieve a conservation law form of the momentum equation which is more convenient from the numerical perspective.

With these simplifications, the KRLNS equations are written

$$\partial_t j_\alpha = -\mathrm{Ma}\partial_\beta\left[j_\alpha j_\beta + \delta_{\alpha\beta}\left(\Theta+\frac{j^2}{2}\right)\right] + \sqrt{\mathrm{Kn}}\partial_\beta\partial_\beta j_\alpha,$$

$$\partial_t\Theta = -\frac{1}{\mathrm{Ma}}\partial_\alpha j_\alpha + \sqrt{\mathrm{Kn}}\partial_\beta\partial_\beta\Theta. \tag{9}$$

The KRLNS equations (9) are valid for $\mathrm{Kn}\ll\mathrm{Ma}\ll 1$, on scales larger than the acoustic scales (5). They can be considered as a simplified computational model of the complete equations, derived in [6]. Note that these simplifications retain the basic physical properties of the equations approaching incompressibility.

III. RESCALING OF VARIABLES

We consider a simplified version of the KRLNS equations (9). First, transform Eq. (9) into the original set of variables (velocity-pressure, $\mathbf{u}$-P), in order to have the same units as AC and INS for a further comparison.

$t'=tt_a$, $\mathbf{x}'=\mathbf{x}L_a$, $\mathbf{j}=\mathbf{m}/(\bar{\rho}U_0)$, $\Theta=\mathcal{G}/(\bar{\rho}U_0^2)$, where

$$t_a = \sqrt{\mathrm{Kn}}\frac{L}{c_s}, \quad L_a = \sqrt{\mathrm{Kn}}L, \tag{10}$$

$\mathcal{G}=P-m^2/2\rho$, $\mathbf{x}=\bar{\rho}\mathbf{u}$, $\mathrm{Kn}=\mu/(\bar{\rho}c_sL)$ (μ is the viscosity coefficient), and finally, the system obtains a dimensionless form by $\mathbf{x}'=\mathbf{x}/L, \mathbf{u}'=\mathbf{u}/U_0, P'=P/\bar{\rho}U_0^2, \mathcal{G}'=\mathcal{G}/(\bar{\rho}U_0^2)$ and usual definition of the Reynolds number $\mathrm{Re}=LU/\nu$.

The resulting system of equations is

$$\partial_t u_\alpha = -\partial_\beta(u_\alpha u_\beta) - \partial_\alpha P + \frac{1}{\mathrm{Re}}\partial_\beta\partial_\beta u_\alpha, \tag{11}$$

$$\partial_t \mathcal{G} = -\frac{1}{\mathrm{Ma}^2}\partial_\alpha u_\alpha + \frac{1}{\mathrm{Re}}\partial_\beta\partial_\beta \mathcal{G}, \tag{12}$$

which provides the coupling between the velocities and the pressure, where P and $\mathcal{G}$ are related as

$$P = \mathcal{G} + \frac{u^2}{2}. \tag{13}$$

Note that Eq. (12) differs from the pressure equation of the AC method (3) by the term $(1/\mathrm{Re})\partial_\beta\partial_\beta\mathcal{G}$. Retaining this term is crucial for capturing the correct time dynamics, as it will be shown in Sec. IV B (see Figs. 4 and 5).

IV. NUMERICAL RESULTS

We are interested in comparing the AC method with the KRLNS approach. Therefore, we discretize both systems using the same numerical method. For this purpose, the explicit MacCormack scheme is used, as proposed in [12]. This method is of predictor-corrector type and is second order accurate both in space and time. In the case of the advection equation

$$\frac{\partial \mathbf{U}}{\partial t} + \frac{\partial \mathbf{F}(\mathbf{U})}{\partial x} + \frac{\partial \mathbf{G}(\mathbf{U})}{\partial y} = 0,$$

where $\mathbf{U}$ is a vector of conserved variables, the explicit MacCormack scheme consists of predictor and corrector steps, respectively:

$$\mathbf{U}^*_{i,j} = \mathbf{U}^n_{i,j} - \frac{\Delta t}{\Delta x}(\mathbf{F}^n_{i+1,j} - \mathbf{F}^n_{i,j}) - \frac{\Delta t}{\Delta y}(\mathbf{G}^n_{i,j+1} - \mathbf{G}^n_{i,j}), \tag{14}$$

$$\mathbf{U}^{n+1}_{i,j} = 0.5\left[\mathbf{U}^n_{i,j} + \mathbf{U}^*_{i,j} - \frac{\Delta t}{\Delta x}(\mathbf{F}^*_{i,j} - \mathbf{F}^*_{i-1,j}) - \frac{\Delta t}{\Delta y}(\mathbf{G}^*_{i,j} - \mathbf{G}^*_{i,j-1})\right]. \tag{15}$$

During the predictor step (14), one-sided forward differences are used in both the x and the y directions. During the corrector step (15), one-sided backward differences are used in both directions. The diffusive terms are discretized with second order central differences in both predictor and corrector step. For example, the term $\partial^2\psi/\partial x^2$ is discretized as

$$\left.\frac{\partial^2\psi}{\partial x^2}\right|^n_{i,j} \approx \frac{\psi^n_{i+1,j} - 2\psi^n_{i,j} + \psi^n_{i-1,j}}{(\Delta x)^2}.$$

The same form is used for the y direction. For the system (11) and (12), $\psi = u, v, \mathcal{G}$, where $u = u_x$ and $v = u_y$. The fully discretized system for the AC method is written in the Appendixes. The system (11) and (12) is now discretized in the same way. In order to ensure numerical stability, the time step suggested in [12] is used:

$$\Delta t \le \frac{0.5\Delta x}{c}.$$

We consider two examples. The first one is the stationary flow in a lid-driven cavity for $\mathrm{Re} = 400, 1000$, and 5000. This example is chosen to demonstrate that the KRLNS equations capture the correct steady-state behavior. Secondly, we compare the numerical solution with one of known exact transient solutions of the incompressible Navier-Stokes equation. This example is chosen to show that the KRLNS equations capture correctly the time behavior, while the AC method does not.

A. Steady-state behavior: Flow in a cavity

The lid-driven cavity problem is a classic CFD test for new methods and numerical algorithms. Let $\Omega = (0,1) \times (0,1)$ be a 2D square cavity, Γ_1 the top boundary, Γ_0 three other sides and $T > 0$ the simulation time. The initial and boundary conditions for the AC method are

$$u_\alpha(x,y) = (1,0), \quad (x,y) \in \Gamma_1, \quad t \in (0,T),$$

$$u_\alpha(x,y) = (0,0), \quad (x,y) \in \Gamma_0, \quad t \in (0,T),$$

$$u_\alpha(x,y) = (0,0), \quad (x,y) \in \Omega, \quad t = 0,$$

$$P(x,y) = 0, \quad (x,y) \in \Omega \cup \Gamma_1 \cup \Gamma_0, \quad t = 0.$$

The boundary values for the artificial pressure equation (3) are taken equal to the values at the adjacent points, i.e.,

$$P_{0,j} = P_{1,j}, \quad 0 \le j \le N-1,$$

$$P_{N-1,j} = P_{N-2,j}, \quad 0 \le j \le N-1,$$

$$P_{i,0} = P_{i,1}, \quad 0 \le i \le M-1,$$

$$P_{i,M-1} = P_{i,M-2}, \quad 0 \le i \le M-1,$$

where N and M are the numbers of grid points in the x and y directions, respectively.

For the KRLNS model, the initial and boundary conditions for the fluid velocity are the same as in the AC method, while for the new pressure equation (12) zero Dirichlet boundary conditions (DBC)

$$P = 0, \quad (x,y) \in \Gamma_0 \cup \Gamma_1 \tag{16}$$

and zero Neumann (NBC)

$$\frac{\partial P}{\partial \mathbf{n}} = 0, \quad (x,y) \in \Gamma_0 \cup \Gamma_1 \tag{17}$$

boundary conditions are used ($\mathbf{n}$ is an exterior normal to the boundary). The realization of the boundary conditions (16) and (17) is according to the formula (13).

The problem is solved by both AC and KRLNS methods, using the same computational grid 256×256. Figure 1 shows the stream functions contours for the cavity flow using the KRLNS equation. We can see that for $\mathrm{Re} = 400, 1000$ the

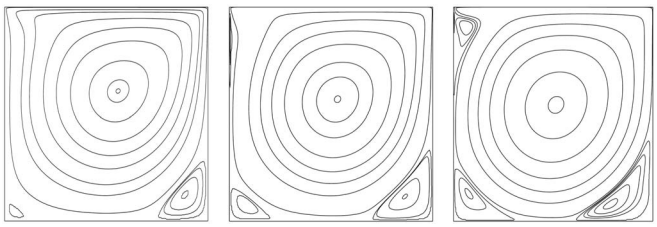

FIG. 1. Streamlines for the cavity flow. Left: Re=400, Ma =0.01; center: Re=1000, Ma=0.01; right: Re=5000, Ma=0.05. Grid 256×256.

method captures the center vortex and two smaller vortices in the right and left bottom corners, and for Re=5000, an additional upper left corner vortex. Figures 2 and 3 present the horizontal and vertical velocity profiles at the cavity's horizontal and vertical centerlines. Excellent agreement between AC and KRLNS methods is seen. Thus Figs. 1–3 demonstrate that the KRLNS method captures the correct quantitative behavior for the steady-state problem. Tables I–IV compare locations of the vortex centers for AC, KRLNS and results available in the literature [13–17].

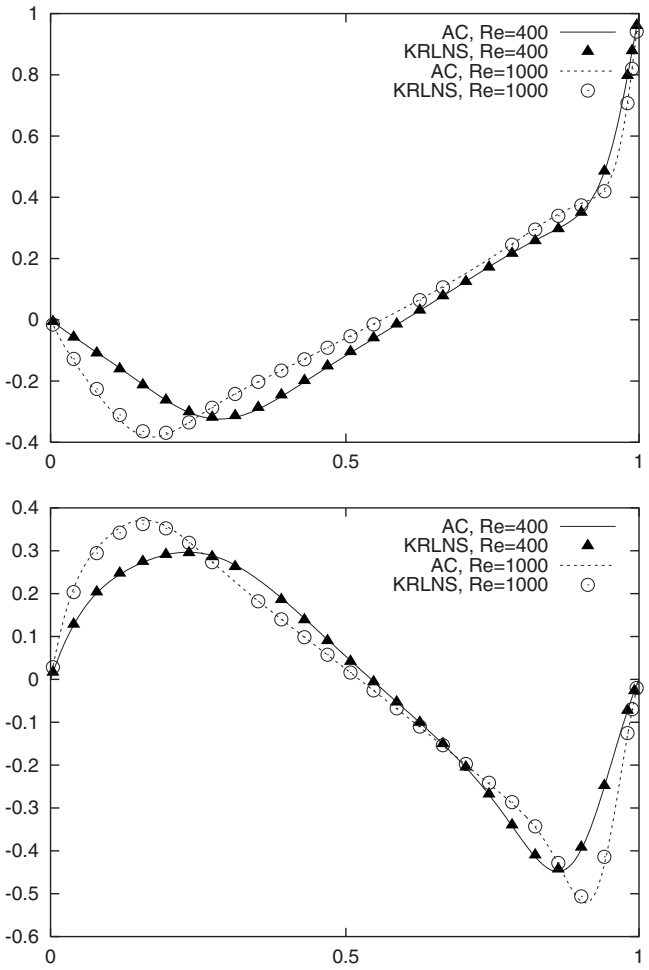

FIG. 2. Comparison for the velocity profiles for the Re=400, 1000. Top: Horizontal velocity, U, at $x=0.5$; bottom: vertical velocity, V, at $y=0.5$. Grid 256×256.

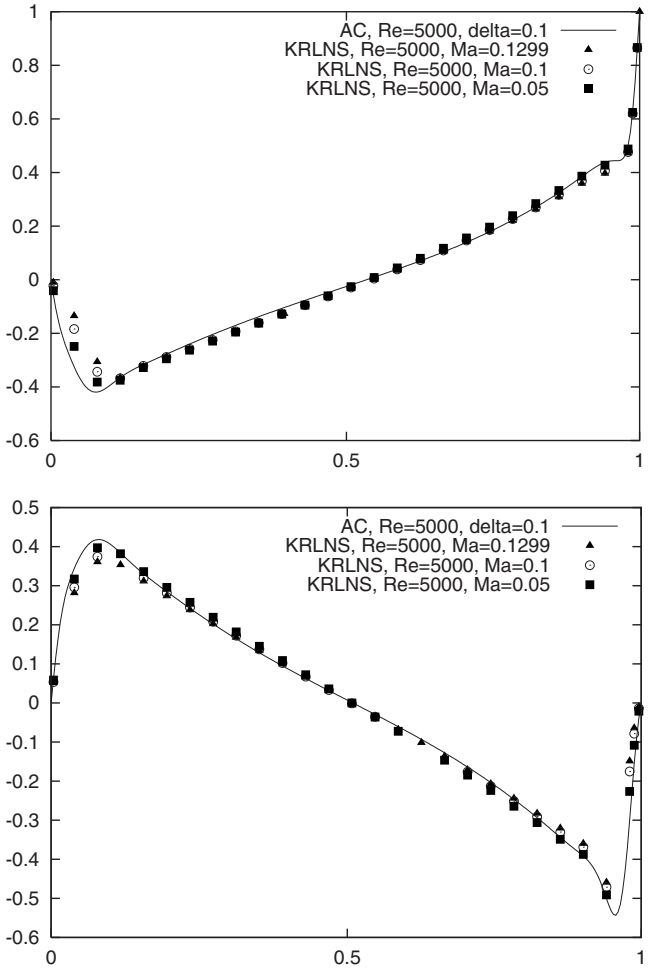

FIG. 3. Comparison for the velocity profiles for the Re=5000 for different values of Ma number. Top: Horizontal velocity, U, at $x=0.5$; bottom: vertical velocity, V, at $y=0.5$. Grid 256×256.

It should be noticed that the numerical results depend essentially on the Mach number. Figure 3 shows the velocity components for Re=5000 and for different values of Ma (Ma=0.1299, 0.1, 0.05). With the decrease of the Mach number, the solution of the KRLNS equations approaches the AC solution.

B. Transient behavior

In order to demonstrate that the KRLNS equation captures the correct time behavior, let us compare the numerical solution with the following exact solution (two-dimensional Taylor-Green vortex flow):

$$u(x,y,t) = -2\pi\phi k_y \cos\left(\frac{2\pi k_x x}{L}\right)\sin\left(\frac{2\pi k_y y}{L}\right) \times \exp\left(-\frac{4\pi^2 k^2 \nu t}{L^2}\right),$$

$$v(x,y,t) = 2\pi\phi k_x \cos\left(\frac{2\pi k_y y}{L}\right)\sin\left(\frac{2\pi k_x x}{L}\right)\exp\left(-\frac{4\pi^2 k^2 \nu t}{L^2}\right),$$

TABLE I. Location of vortex centers in a lid driven cavity flow, Re=400.

Ref.	Primary vortex $(x,y,\psi_{\max})$	Lower right vortex $(x,y,\psi_{\min}\times 10^4)$	Lower left vortex $(x,y,\psi_{\min}\times 10^5)$
[13], Ma=0.1732	(0.5608,0.6078,0.1121)	(0.8902,0.126,−6.19)	(0.0549,0.0510,−1.30)
[14]	(0.5547,0.6055,0.1139)	(0.8906,0.125,−6.42)	(0.0508,0.0469,−1.42)
[15], Ma=0.1299	(0.5573,0.6049,0.1127)	(0.8854,0.122,−6.09)	(0.0392,0.0353,−1.2)
[16]	(0.5563,0.6000,0.1136)	(0.8875,0.119,−6.45)	(0.0500,0.0500,−1.46)
Present work, AC, δ=0.01	(0.5608,0.6118,0.1125)	(0.8883,0.1294,−6.2)	(0.0549,0.0510,−1.0)
Present work, DBC KRLNS, Ma=0.01	(0.5608,0.6118,0,1116)	(0.8902,0.1255,−6.2)	(0.0549,0.051,−1.0)
Present work, NBC KRLNS, Ma=0.01	(0.5608,0.6078,0,1134)	(0.8902,0.1255,−6.6)	(0.0588,0.051,−1.0)

TABLE II. Location of vortex centers in a lid driven cavity flow, Re=1000.

Ref.	Primary vortex $(x,y,\psi_{\max})$	Lower right vortex $(x,y,\psi_{\min}\times 10^4)$	Lower left vortex $(x,y,\psi_{\min}\times 10^5)$
[13], Ma=0.1732	(0.5333,0.5647,0.1178)	(0.8667,0.114,−16.9)	(0.0902,0.0784,−22.2)
[14]	(0.5313,0.5625,0.1179)	(0.8594,0.110,−17.5)	(0.0859,0.0781,−23.1)
[15], Ma=0.1299	(0.5338,0.5675,0.1178)	(0.8654,0.115,−16.8)	(0.0882,0.0797,−21.8)
[15], Ma=0.1732	(0.5338,0.5648,0.1178)	(0.8654,0.115,−16.7)	(0.0855,0.0797,−21.6)
[16]	(0.5438,0.5625,0.1173)	(0.8625,0.106,−17.4)	(0.0750,0.0813,−22.4)
Present work, AC, δ=0.01	(0.5333,0.5686,0.1172)	(0.8667,0.1176,−17)	(0.0863,0.0823,−22)
Present work, DBC KRLNS, Ma=0.01	(0.5333,0.5725,0.1154)	(0.8627,0.1137,−18)	(0.0863,0.0823,−20)
Present work, NBC KRLNS, Ma=0.01	(0.5373,0.5686,0,1175)	(0.8667,0.1137,−18.5)	(0.0863,0.0784,−21)

TABLE III. Location of vortex centers in a lid driven cavity flow, Re=5000.

Ref.	Primary vortex $(x,y,\psi_{\max})$	Lower right vortex $(x,y,\psi_{\min}\times 10^4)$	Lower left vortex $(x,y,\psi_{\min}\times 10^5)$
[13] Ma=0.1732	(0.5176,0.5373,0.1214)	(0.8078,0.075,−30.3)	(0.0784,0.1373,−135)
[14]	(0.5117,0.5352,0.1190)	(0.8086,0.074,−30.8)	(0.0703,0.1367,−136)
[15], Ma=0.1299	(0.5175,0.5350,0.1204)	(0.8056,0.072,−30.1)	(0.0773,0.136,−134)
[16]	(0.5125,0.5313,0.0921)	(0.8500,0.081,−54.9)	(0.0625,0.1563,−167)
Present work, AC, δ=0.1	(0.5176,0.5412,0.1081)	(0.8039,0.0784,−31.3)	(0.0784,0.1373,−129)
Present work, DBC KRLNS, Ma=0.05	(0.5176,0.5451,0.1107)	(0.7922,0.0824,−32.6)	(0.0784,0.1333,−107)

TABLE IV. Location of the upper left vortex centers in a lid driven cavity flow, Re=5000.

Ref.	$(x, y, \psi_{\min} \times 10^3)$
[13], Ma=0.1732	(0.0667, 0.9059, −1.40)
[14]	(0.0625, 0.9102, −1.4564)
Present work, AC, δ=0.1	(0.0667, 0.9137, −1.31)
Present work, KRLNS, Ma=0.05	(0.0667, 0.9137, −1.45)

$$p(x,y,t) = -\pi^2\phi^2\left[k_y^2\cos\left(\frac{4\pi k_x x}{L}\right) + k_x^2\cos\left(\frac{4\pi k_y y}{L}\right)\right] \times \exp\left(-\frac{8\pi^2 k^2 \nu t}{L^2}\right)$$

on the domain $[0,\pi]\times[0,\pi]$ ($L=\pi$) at Re=1. Here $k^2=k_x^2+k_y^2$. The following parameters are used: $k_x=k_y=0.5$, $\phi=1/\pi$, and $\nu=1$.

Figures 4 and 5 (top) compare the pressure component for AC, KRLNS and the exact solution of the INS equation for the grids 32×32 and 64×64. An excellent agreement between the pressure component of the numerical solution of the KRLNS equation and the exact solution of the INS equation is seen. The AC approach provides us with the oscillating pressure component.

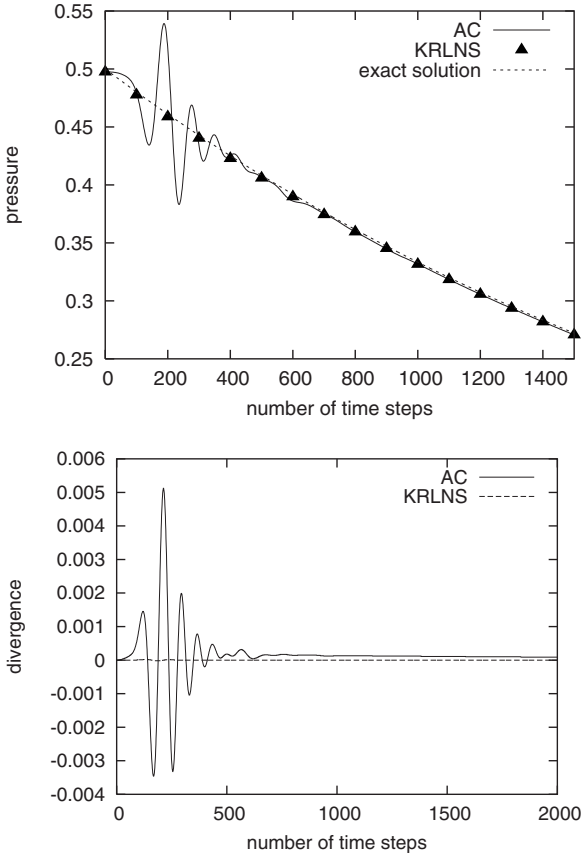

FIG. 4. Top: Pressure as a function of time for δ=0.0001. Bottom: Divergence as a function of time for δ=0.0001. Re=1, Ma=0.01, and $\Delta t=10^{-4}$. Grid 32×32.

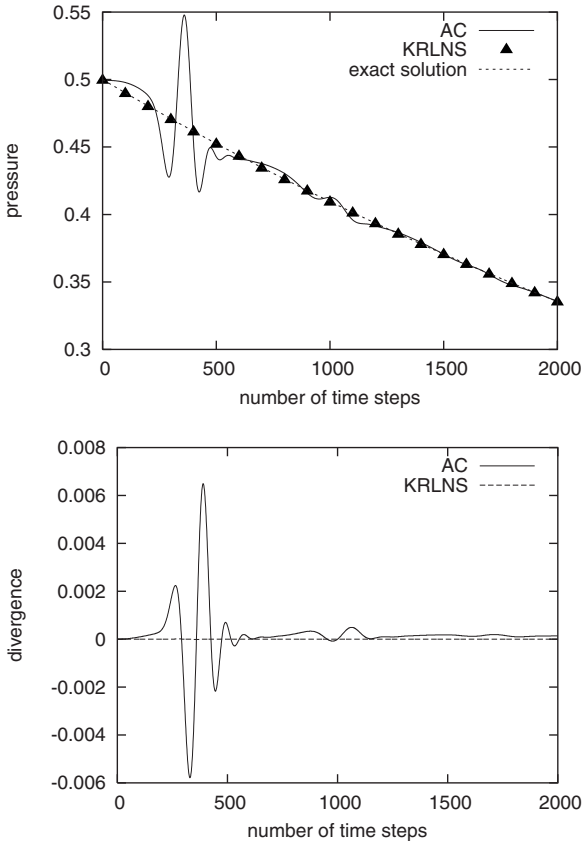

FIG. 5. Top: Pressure as a function of time for δ=0.0001. Bottom: Divergence as a function of time for δ=0.0001. Re=1, Ma=0.01, and $\Delta t=5\times10^{-5}$. Grid 64×64.

Figures 4 and 5 (bottom) depict the divergence history for AC and KRLNS for the grids 32×32 and 64×64. It can be seen that the $\partial_\alpha u_\alpha$ term for the KRLNS model holds at the zero level, while the divergence in the AC method oscillates. The calculation is performed at a constant Courant number: $\Delta t/\Delta x=10^{-3}$.

The oscillations in the AC solution are due to absence of a smoothing effect in the model. Such an effect in the KRLNS is provided by the additional term (proportional to 1/Re) in Eq. (12). It should be noted here that the oscillatory behavior of the AC method shown in Fig. 5 is a general feature of the method and does not disappear for smaller values of δ. If we decrease the value of delta, then the oscillations are compressed towards $t=0$ but they still do not entirely disappear. This behavior is shown in Fig. 6.

Figure 7 demonstrates component-wise comparison of the velocity profiles at various times vs. analytical sinusoidal profile.

Notice that in [7] oscillations of divergence of order Ma on the time scale of order Ma were detected. Figures 4 and 5 (bottom) do not show these oscillations.

V. CONCLUSION

The present study is concerned with the numerical solutions of the KRLNS equation suggested in [6] and its com-

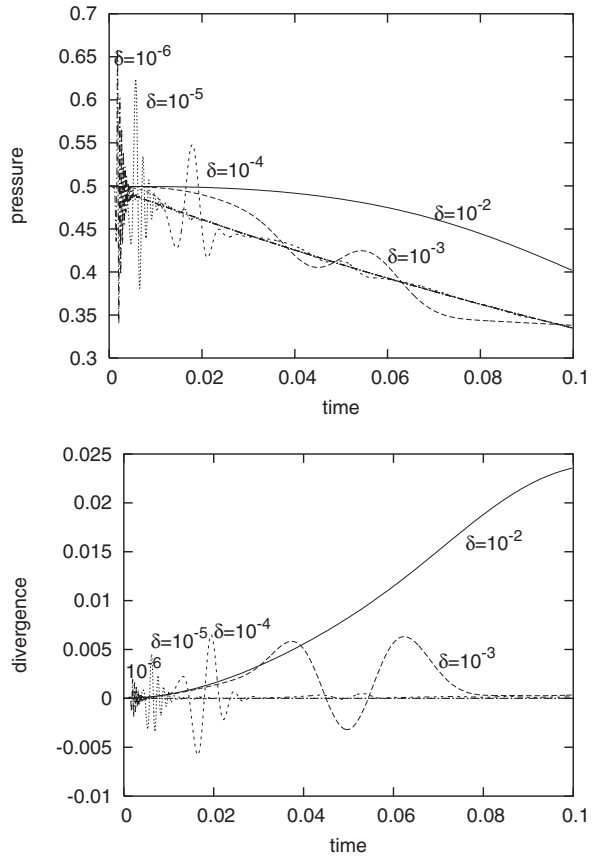

FIG. 6. Top: Pressure as a function of time for different values of δ for the AC method. Bottom: Divergence as a function of time for different values of δ. Re=1 and Ma=0.01. Grid 64×64.

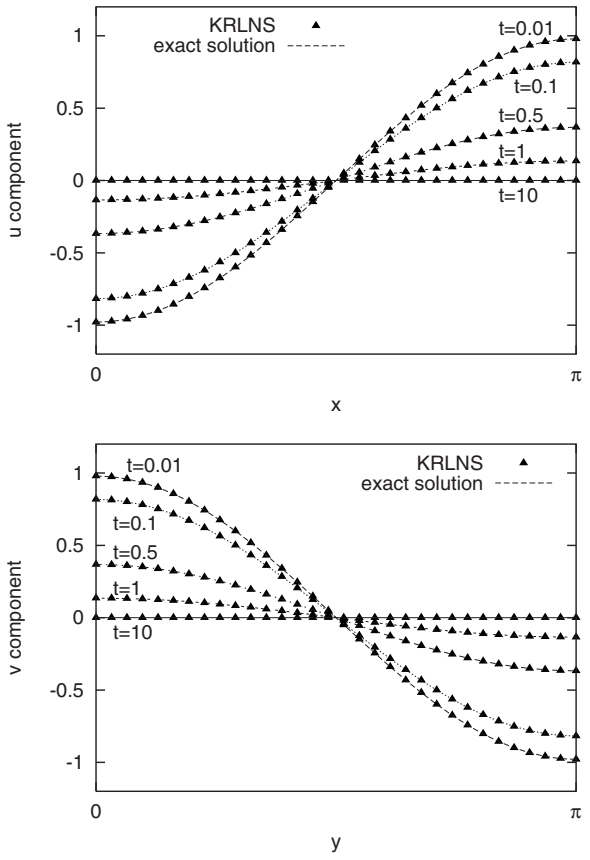

FIG. 7. Comparison of the velocity profiles for KRLNS at various times vs analytical sinusoidal profile. Top: $u(x,\pi/2,t)$; bottom: $v(\pi/2,y,t)$. Grid 32×32.

parison with the AC method [8]. In spite of the superficial similarity of the artificial pressure equation (3) and the corresponding pressure equation of the AC method (12) there are at least two significant differences. First, Eq. (12) contains additional dissipation term (proportional to $1/\mathrm{Re}$), which cannot be neglected, as removing this term will change a qualitative behavior of the system (see Figs. 4 and 5). In fact, this term is the main difference of the physical KRLNS model from the AC model. Secondly, while the original AC method fails to capture time dynamics correctly, the current method can do so. This fact is demonstrated by the example in Sec. IV B.

The flow in a cavity problem is solved in a framework of the new approach using a simple explicit MacCormack method. A comparison with the results available from the literature for this benchmark test indicates that the KRLNS method is an alternative approach to study motion of incompressible fluids at low Mach numbers.

Finally, in Appendix B we demonstrate that the Jacobian matrices of fluxes in the KRLNS system have real eigenvalues and are diagonalizable. A well known route to numerically solve such systems is to use characteristics based methods (see, e.g., [19,20]). One of the recently developed methods is Numerical Acoustic Relaxation (NAR) method [18], which will be considered in our future work.

ACKNOWLEDGMENTS

S.B. and S.A. kindly acknowledge the support from NTU Office of Research (SUG project 58120006). I.V.K. gratefully acknowledges support by BFE Project 100862 and by CCEM-CH.

APPENDIX A: NUMERICAL METHOD

For the artificial compressibility method we have the following ($u=u_x$, $v=u_y$).

(1) Predictor step

$$u^*_{i,j} = u^n_{i,j} - c_1[(u^n_{i+1,j})^2 - (u^n_{i,j})^2] - c_2[u^n_{i,j+1}v^n_{i,j+1} - u^n_{i,j}v^n_{i,j}] - c_1[P^n_{i+1,j} - P^n_{i,j}] + c_3[u^n_{i+1,j} - 2u^n_{i,j} + u^n_{i-1,j}] + c_4[u^n_{i,j+1} - 2u^n_{i,j} + u^n_{i,j-1}], \quad \text{(A1)}$$

$$v^*_{i,j} = v^n_{i,j} - c_1[u^n_{i+1,j}v^n_{i+1,j} - u^n_{i,j}v^n_{i,j}] - c_2[(v^n_{i,j+1})^2 - (v^n_{i,j})^2] - c_2[P^n_{i,j+1} - P^n_{i,j}] + c_3[v^n_{i+1,j} - 2v^n_{i,j} + v^n_{i-1,j}] + c_4[v^n_{i,j+1} - 2v^n_{i,j} + v^n_{i,j-1}], \quad \text{(A2)}$$

$$P^*_{i,j} = P^n_{i,j} - \frac{1}{\delta}(c_1[u^n_{i+1,j} - u^n_{i,j}] + c_2[v^n_{i,j+1} - v^n_{i,j}]). \quad \text{(A3)}$$

For the KRLNS system (11)–(13), the flow velocities equations are discretized in the same way. For the grand potential equation (12) we have

$$\mathcal{G}^*_{i,j} = \mathcal{G}^n_{i,j} - \frac{1}{\mathrm{Ma}^2}(c_1[u^n_{i+1,j} - u^n_{i,j}] + c_2[v^n_{i,j+1} - v^n_{i,j}]) + c_3[\mathcal{G}^n_{i+1,j} - 2\mathcal{G}^n_{i,j} + \mathcal{G}^n_{i-1,j}] + c_4[\mathcal{G}^n_{i,j+1} - 2\mathcal{G}^n_{i,j} + \mathcal{G}^n_{i,j-1}]. \tag{A4}$$

(2) Corrector step

$$u^{n+1}_{i,j} = 0.5\{u^*_{i,j} + u^n_{i,j} - c_1[(u^*_{i,j})^2 - (u^*_{i-1,j})^2] - c_2[u^*_{i,j}v^*_{i,j} - u^*_{i,j-1}v^*_{i,j-1}] - c_1[P^*_{i,j} - P^*_{i-1,j}] + c_3[u^*_{i+1,j} - 2u^*_{i,j} + u^*_{i-1,j}] + c_4[u^*_{i,j+1} - 2u^*_{i,j} + u^*_{i,j-1}]\}, \tag{A5}$$

$$v^{n+1}_{i,j} = 0.5\{v^*_{i,j} + v^n_{i,j} - c_1[u^*_{i,j}v^*_{i,j} - u^*_{i-1,j}v^*_{i-1,j}] - c_2[(v^*_{i,j})^2 - (v^*_{i,j-1})^2] - c_2[P^*_{i,j} - P^*_{i,j-1}] + c_3[v^*_{i+1,j} - 2v^*_{i,j} + v^*_{i-1,j}] + c_4[v^*_{i,j+1} - 2v^*_{i,j} + v^*_{i,j-1}]\}, \tag{A6}$$

$$P^{n+1}_{i,j} = 0.5\left[P^*_{i,j} + P^n_{i,j} - \frac{1}{\delta}(c_1[u^*_{i,j} - u^*_{i-1,j}] + c_2[v^*_{i,j} - v^*_{i,j-1}])\right]. \tag{A7}$$

For the KRLNS grand potential equation we have

$$\mathcal{G}^{n+1}_{i,j} = 0.5 * \left[\mathcal{G}^*_{i,j} + \mathcal{G}^n_{i,j} - \frac{1}{\mathrm{Ma}^2}(c_1[u^*_{i,j} - u^*_{i-1,j}] + c_2[v^*_{i,j} - v^*_{i,j-1}]) + c_3[\mathcal{G}^*_{i+1,j} - 2\mathcal{G}^*_{i,j} + \mathcal{G}^*_{i-1,j}] + c_4[\mathcal{G}^*_{i,j+1} - 2\mathcal{G}^*_{i,j} + \mathcal{G}^*_{i,j-1}]\right], \tag{A8}$$

where

$$c_1 = \frac{\Delta t}{\Delta x}, \quad c_2 = \frac{\Delta t}{\Delta y}, \quad c_3 = \frac{\Delta t}{\mathrm{Re}(\Delta x)^2}, \quad c_4 = \frac{\Delta t}{\mathrm{Re}(\Delta y)^2}.$$

Notice that we are not provided with boundary conditions for the grand potential $\mathcal{G}$, but for the pressure P. After the calculation is done for the inner points of the grid by formulas (A4) and (A8), the values on the boundary are completed with the help of formula (13).

APPENDIX B: CHARACTERISTIC ANALYSIS

In this section we demonstrate that the Jacobian matrices of fluxes in the KRLNS system have real eigenvalues and are diagonalizable. Let us rewrite the system (11)–(13) in the conservative form. For the two-dimensional case we have

$$\partial_t \mathbf{U} + \partial_x \mathbf{F} + \partial_y \mathbf{G} = \mathbf{S}, \tag{B1}$$

where $\mathbf{U},\mathbf{F},\mathbf{G},\mathbf{S}$ are vectors of conservative variables, fluxes, and source term, respectively:

$$\mathbf{U} = \begin{bmatrix} \mathcal{G} \\ u_x \\ u_y \end{bmatrix}, \quad \mathbf{F} = \begin{bmatrix} \frac{1}{\mathrm{Ma}^2}u_x \\ u_x^2 + P \\ u_x u_y \end{bmatrix}, \quad \mathbf{G} = \begin{bmatrix} \frac{1}{\mathrm{Ma}^2}u_y \\ u_x u_y \\ u_y^2 + P \end{bmatrix},$$

$$\mathbf{S} = \begin{bmatrix} \frac{1}{\mathrm{Re}}\partial_\beta\partial_\beta\mathcal{G} \\ \frac{1}{\mathrm{Re}}\partial_\beta\partial_\beta u_x \\ \frac{1}{\mathrm{Re}}\partial_\beta\partial_\beta u_y \end{bmatrix}. \tag{B2}$$

The Jacobian matrices for fluxes $\mathbf{F},\mathbf{G}$ are

$$\mathbf{J_F} = \begin{bmatrix} 0 & \frac{1}{\mathrm{Ma}^2} & 0 \\ 1 & 3u_x & u_y \\ 0 & u_y & u_x \end{bmatrix}, \quad \mathbf{J_G} = \begin{bmatrix} 0 & 0 & \frac{1}{\mathrm{Ma}^2} \\ 0 & u_y & u_x \\ 1 & u_x & 3u_y \end{bmatrix}. \tag{B3}$$

Characteristic equation of the matrix $\mathbf{J_F}$ is

$$\lambda^3 - 4u_x\lambda^2 + \lambda\left(3u_x^2 - u_y^2 - \frac{1}{\mathrm{Ma}^2}\right) + \frac{u_x}{\mathrm{Ma}^2} = 0.$$

Discriminant of this equation is $D = p^3/27 + q^2/4$, where

$$p = -\left(\frac{7}{3}u_x^2 + u_y^2 + \frac{1}{\mathrm{Ma}^2}\right), \quad q = -u_x\frac{9 + 4\,\mathrm{Ma}^2(5u_x^2 + 9u_y^2)}{27\,\mathrm{Ma}^2}.$$

It is easy to verify that $D < 0$. This means that the characteristic equation has three real nonequal roots. The roots can be written as

$$\lambda_1 = \frac{4}{3}u_x + 2\sqrt{\frac{|p|}{3}}\cos\frac{\phi}{3}, \tag{B4}$$

$$\lambda_2 = \frac{4}{3}u_x - 2\sqrt{\frac{|p|}{3}}\cos\frac{\phi + \pi}{3}, \tag{B5}$$

$$\lambda_3 = \frac{4}{3}u_x - 2\sqrt{\frac{|p|}{3}}\cos\frac{\phi - \pi}{3}, \tag{B6}$$

where

$$\phi = \arccos\left[-\frac{q}{2\sqrt{\frac{|p|^3}{27}}}\right].$$

The roots of the characteristic equation for the matrix $\mathbf{J_G}$ can be found in a similar way. Thus the matrices $\mathbf{J_F}$ and $\mathbf{J_G}$ have three real nondegenerate eigenvalues and therefore are diagonalizable.

[1] L. D. Landau and E. M. Lifshitz, *Fluid Mechanics* (Pergamon Press, Oxford, 1987).
[2] F. Higuera, S. Succi, and R. Benzi, Europhys. Lett. **9**, 345 (1989).
[3] X. Shan and X. He, Phys. Rev. Lett. **80**, 65 (1998).
[4] S. Ansumali and I. V. Karlin, Phys. Rev. Lett. **95**, 260605 (2005).
[5] H. Chen, S. Kandasamy, S. Orszag, R. Shock, S. Succi, and V. Yakhot, Science **301**, 633 (2003).
[6] S. Ansumali, I. V. Karlin, and H. C. Ottinger, Phys. Rev. Lett. **94**, 080602 (2005).
[7] I. V. Karlin, A. G. Tomboulides, C. E. Frouzakis, and S. Ansumali, Phys. Rev. E **74**, 035702(R) (2006).
[8] A. J. Chorin, J. Comput. Phys. **2**, 12 (1967).
[9] S. E. Rogers and D. Kwak, Appl. Numer. Math. **8**, 43 (1991).
[10] S. E. Rogers and D. Kwak, AIAA J. **28**, 253 (1990).
[11] C. Kiris and D. Kwak, Comput. Fluids **31**, 627 (2002).
[12] A. Perrin and H. H. Hu, J. Comput. Phys. **212**, 166 (2006).
[13] S. Hou, J. Comput. Phys. **118**, 329 (1995).
[14] U. Ghia, K. N. Ghia, and C. Y. Shin, J. Comput. Phys. **48**, 387 (1982).
[15] S. Ansumali, *Minimal Kinetic Modeling of Hydrodynamics* (Diss. ETH No 15534, 2004).
[16] S. P. Vanka, J. Comput. Phys. **65**, 138 (1982).
[17] C.-H. Bruneau and M. Saad, Comput. Fluids **35**, 326 (2006).
[18] R. R. Nourgaliev, T. N. Dinh, and T. G. Thenofanous, Int. J. Multiphase Flow **30**, 901 (2004).
[19] R. J. Le Veque, *Numerical Methods for Conservation Laws* (Birkhauser-Verlag, Basel, 1992).
[20] A. Bardow, I. V. Karlin, and A. A. Gusev, Europhys. Lett. **75**, 434 (2006).